Sensors & Actuators: A. Physical 359 (2023) 114496

Contents lists available at ScienceDirect

Sensors and Actuators: A. Physical

journal homepage: www.journals.elsevier.com/sensors-and-actuators-a-physical

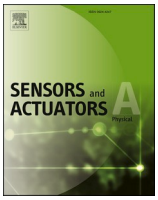

Rapid prototyping Lab-on-Chip devices for the future: A numerical optimisation of bulk optical parameters in microfluidic systems

Sarah E. Lu [a,*], Andrew Morris [b], Geraldine Clinton-Bailey [b], Medya Namiq [c], Paul C. Gow [c], Antony Birchill [b,d], Sebastian Steigenberger [b], James Wyatt [b], Reuben Forrester [b], Matthew C. Mowlem [b], Phillip E. Warwick [a]

[a] University of Southampton, National Oceanography Centre, European Way, Southampton SO14 3ZH, UK
[b] Ocean Technology and Engineering Group, National Oceanography Centre, Southampton SO14 3ZH, UK
[c] Optoelectronics Research Centre, University of Southampton, Southampton SO17 1BJ, UK
[d] School of Environment, Geography and Geosciences, University of Portsmouth, PO1 2UP, UK

ARTICLE INFO

Keywords:
Lab on Chip
Ray tracing
Optical modelling
Global warming
Radionuclides
Nuclear industry

ABSTRACT

Nuclear reactor process control is typically monitored for pure β-emitting radionuclides via manual sampling followed by laboratory analysis, leading to delays in data availability and response times. The development of an in situ microfluidic Lab on Chip (LoC) system with integrated detection capable of measuring pure β-emitting radionuclides presents a promising solution, enabling a reduction in occupational exposure and cost of monitoring whilst providing improved temporal resolution through near real-time data acquisition. However, testing prototypes with radioactive sources is time-consuming, requires specialist facilities/equipment, generates contaminated waste, and cannot rapidly evaluate a wide range of designs or configurations. Despite this, modelling multiple design parameters and testing their impact on detection with non-radioactive substitutes has yet to be adopted as best practice. The measurement of pure β emitters in aqueous media relies on the efficient transport of photons generated by the Cherenkov effect or liquid scintillators to the detector. Here we explore the role of numerical modelling to assess the impact of optical cell geometry and design on photon transmission and detection through the microfluidic system, facilitating improved designs to realise better efficiency of integrated detectors and overall platform design. Our results demonstrate that theoretical modelling and an experimental evaluation using non-radiogenic chemiluminescence are viable for system testing design parameters and their impact on photon transport. These approaches enable reduced material consumption and requirement for specialist facilities for handling radioactive materials during the prototyping process. This method establishes proof of concept and the first step towards numerical modelling approaches for the design optimisation of microfluidic LoC systems with integrated detectors for the measurement of pure β emitting radionuclides via scintillation-based detection.

1. Introduction

The development of in situ technology capable of detecting pure β-emitting radionuclides is extremely attractive for applications in the nuclear industry. This technology presents the opportunity for autonomous collection of spatially and temporally resolved data, improving the accuracy of real-time process control in nuclear power plants (NPP) and processing facilities (NPF) to maintain system integrity and minimise out-of-core radiation fields [1]. In this context, in situ Lab on Chip (LoC) systems have the potential to reduce operator exposure and minimise the production of contaminated waste through the reduced use of samples and reagents [2,3]. Integrating LoC technology will also reduce manual sampling, which has additional risks and costs, including; sample degradation, contamination, and the need for sample preservation during transportation [4].

LoC radiometric detection for NPFs and NPPs is an emergent field, and best practices for technology development have yet to be established. Presently, reported LoC radiochemical platforms integrated with

* Correspondence to: The School of Ocean and Earth Science, Faculty of Environmental and Life Science, University of Southampton, National Oceanography Centre, Waterfront Campus, European Way, Southampton S014 3ZH, UK.
E-mail address: Sarah.Lu@soton.ac.uk (S.E. Lu).

https://doi.org/10.1016/j.sna.2023.114496
Received 17 August 2022; Received in revised form 10 June 2023; Accepted 13 June 2023
Available online 14 June 2023

detectors have concentrated on radiotracer synthesis and analysis, which focus on short-lived (a half-life of minutes to hours) radionuclides that decay to non-radioactive daughter products. Miniaturised radiochemical applications, in particular devices for radiopharmaceutical synthesis [5–10] and quality control [11–14], radiobioassay [15], and radionuclide separation for nuclear fuel [16–18], are already well summarised [7,8,19–28].

Typical LoC systems consist of three pieces of hardware: a microfluidic chip, a fluid control system such as pumps and connective tubing, and a detector [15]. The most common radiometric LoCs detection method is optical, utilising either the Cherenkov effect or scintillation-based methods for photon production [29–32]. Factors affecting overall sensor efficiency, including detector performance [12], scintillator efficiency [33,34], and microfluidic chip materials [13], have already been considered elsewhere [13,14,35,36]. Cho et al. previously [37] assessed the impact of channel geometry on overall sensor efficiency in the context of a radiometric LoC system for ^{18}F-labeled compounds. A channel spacing of at least 1.0 mm was required to accommodate the spatial resolution of the charge-coupled device (CCD) [37]. Here we have explored the optimisation of a single straight channel design, the assessment was expanded to include combinations and variations of key design parameters such as channel width, height and coatings. Modelled width and coating parameters were then compared to experimental evaluation to begin the coupling of modelling photon detection-based microfluidic systems and radiological systems.

To date, radiometric LoC detection efficiency has typically been optimised through prototype development and particle penetrability simulations [13,30,31] utilising Monte Carlo N-Particle (MCNP) Transport Code or GEANT4 [38]. Both are general-purpose, continuous-energy, generalized-geometry, time-dependent, radiation transport codes designed to track many particle types over broad ranges of energies to simulate the passage of particles through matter. However, both MCNP and GEANT4 lack the capacity for assessing optical collection methods alongside simulated particle paths. Numerical modelling applications have been utilised for radionuclide separation [39–41], with computer automated design demonstrating potential alternatives to immediate prototyping. Finite element analysis (FEA) packages have previously been used to model fluid mechanics in various systems [42–45] to optimise mixing, separation, and bioparticle focusing. So far, optimisation of optical detection efficiency by modelling key design parameters prior to prototyping remains unexplored as a means of directing areas of development for LoC systems that rely on photon collection for radiometric analysis [13,30–32].

The average benchtop instrumental detection efficiency of Cherenkov photons over the spectral range of visible light is $\varepsilon = 0.1$ [46]. For radiometric LoC systems where small sample volumes limit Cherenkov photon yield, it is vital to reduce photon loss by optimising channel design and reducing photon loss at the detector channel interface [47,48]. The use of radiogenic material in prototyping radiometric LoC devices also carries additional material, labour, and fabrication costs. Radionuclides of industrial interest generally possess half-lives ranging from days to years, often taking multiple disintegrations to reach stable nuclides. Disposal of contaminated prototypes results in prohibitive costs inhibiting the exploration of novel design features. For successful rapid prototyping, models must be affordable to build and run; therefore, establishing an accurate model with the simplest parameters is critical.

Numerical modelling currently supports the frontier development and application of various scientific and engineering disciplines. There are many numerical modelling and ray-tracing methods that have been developed based on established modelling techniques for luminescence in microfluidic or portable systems [49–54]. These methods include applications for analytes of environmental[43,55,56], clinical [49,50,52,57], and forensic interest [53]. Here we present the foundations of best practices for developing novel radiometric prototypes. Our method can be used to examine the interplay between different parameters in a radiometric microfluidic system, including dimensions, surface area, materials, and surface reflectivity. We demonstrate the validity of this model using a similar experimental setup employing the luminol-peroxide chemiluminescence (CL) reaction as a substitute for photon production that would otherwise be produced from Cherenkov radiation. Both processes have a medium that is overwhelmingly water and produce continuous spectra in the blue visible light region. The luminol peroxide CL produces continuous but time variant photons allowing the bulk optical properties of the flow cell to be examined with a flowing analyte. Together these findings demonstrate that numerical modelling can be used as an economical and rapid prototyping method for trending optical outputs in developing novel LoC devices. This approach can be applied to many LoC applications that rely on direct photon detection or CL, enabling the most promising novel designs to be evaluated before development and investment without needing specialist facilities.

2. Finite element analysis of microfluidic system

COMSOL Multiphysics® software was used to perform photon transport modelling [50] through the microfluidic channel using the Ray Tracing Optics module. Photon release was simulated and analysed (Fig. 1a) in a single idealised microfluidic channel with a detector directly overhead and separated from the channel by a Poly(methyl methacrylate) (PMMA) spacer (Fig. 1b).

The configuration simulates a sample being held in the microfluidic channel under the detector. Photons must pass through the channel and spacer to strike the detector, modelled as a 2D plane. The detector dimensions are based on the Hamamatsu (type H10492–011) Photomultiplier tube (PMT) detection window, which was selected for its spectral response range of 300–850 nm as a direct comparison to the experimental setup. This detector also represents the type and size likely to be employed in a final LoC radiological sensor looking at photon release resulting from β emission.

Most microfluidic radionuclide detector prototypes place the detector on top of the microfluidic channels [13,30,34,35] to expose the detector to as much fluid surface area as possible. In contrast, some High Energy Physics (HEP) applications have successfully placed the multi-anode PMTs perpendicular to metallised channels acting as optical waveguides [31,32]. Devices developed for spatial resolution within the microfluidic channel place detectors at the end and experience considerable photon loss along the channel length [48], which is not a target of this study, so it has not been explored further in this work.

2.1. Physical components of the modelled system

Global dimensions and geometries of the model are summarised in Table S.1. The range of simulated channel dimensions was selected according to current manufacturing capabilities for CNC milling, solvent processing, and pressure bonding. The channel dimensions also maintain laminar flow and adequate fluidic dispersion suppression within a rectangular microfluidic channel (Table S.2). Channel height and width were increased by 0.1 mm in isolation for each model dimension simulated to ensure adequate increase in detector output which can be compared by an analogous experimental system.

For all models, each material used its refractive index at 420 nm wavelength (peak of Cherenkov emission spectrum [46]). Typical extinction coefficients and the optical densities of the materials were used throughout all models [58]. The channel's media was water (RI 1.33), and the absorption coefficient is considered negligible at 420 nm. All models were simulated with an opaque surface (reflection coefficient 0.04) or reflective surface (reflection coefficient 0.96) behind the channel wall. A reflection coefficient of 1 was not used in the reflective system to account for potential defects in an experimental setup. The detector's quantum efficiency was maintained as 1, and the noise was not modelled as the performance of the detector is not the focus of this

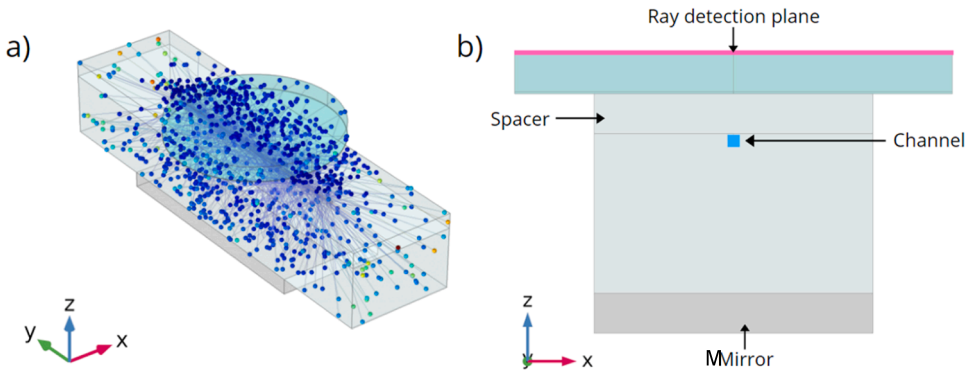

Fig. 1. a) Ray tracing over entire model b) labelled cross-section of the model, the channel is not to scale.

work. Mesh and boundary conditions specific to the geometrical optics system is available in the supplementary information.

All results are assessed relative to a baseline to enable direct comparisons across the various parameters to be investigated. The baseline case has a channel width and height of 0.3 mm, length of 30 mm, and spacer thickness of 2 mm with an opaque backing (Fig. 1b).

2.2. Photon production and release parameters

The pure β emitter ^{90}Sr with a maximum energy of 546 KeV was selected as the target radionuclide for the modelled system because of its capability to emit a significant abundance of high-energy β particles through its progeny ^{90}Y compared to other pure β emitting radionuclides of interest (e.g. ^{3}H, ^{99}Tc). Its daughter nuclei ^{90}Y has a shorter half-life of 64 h and decays itself via a maximum 2282 KeV beta emission into stable ^{90}Zr. The short half-life of ^{90}Y means that it is often found in secular equilibrium with ^{90}Sr.

The average kinetic energy of a β particle emitted from ^{90}Sr is ~ 182 keV; below the Cherenkov threshold energy of 264 keV in water, whilst the average energy (E_{avg})of a β particle emitted from ^{90}Y is ~760 keV. Therefore, most Cherenkov photons produced will be from a ^{90}Y β particle emission, and a small proportion arising from β particles emitted from ^{90}Sr with above average kinetic energy. The number of photons (N) emitted for a single β particle produced within the sample volume was estimated with the Frank Tamm equation:$N = 2\pi\alpha x(1/\lambda_2 - 1/\lambda_1)(\sin^2\theta_c)$, where λ_1 and λ_2 are the upper and lower limits of the selected wavelength region, respectively, α is the fine structure constant, θ_c is the Cherenkov emission angle dependent on the emitted β particle energy, and x is the particle path length. The spectral region was defined as $3.0x10^{-5}$ and $8.5x10^{-5}$ cm. For ^{90}Y emitting a single β particle of E_{avg} with a maximum possible path length (x) of 0.3 cm in water, 90 photons are produced (without deceleration of the β particle).

To guarantee the participation of optical edge case scenarios in the channel and to eliminate the number of photons acting as a variable, the number of photons was scaled by a factor of 10, equivalent to 3.7 KBqmL^{-1} for the 0.3 mm channel case. The number of photons was then increased proportionally to channel volume, ensuring the activity in the channel was kept constant. It was assumed that no Cherenkov photons were produced in the PMMA surrounding the channel.

In COMSOL [59], release parameters (defined in Table S.5) used a *domain release* with an *initial position* based on a density ρ proportional to 1 (based on the overwhelming channel contents, which is water). The *release distribution accuracy order* was set to 5 and the *position refinement factor* to 10. Ray direction vector (*mode of release*) was set to spherical to account for any potential direction of the Cherenkov emission cone. The *number of photons in the wave vector space nw* was set to 1, and the *distribution* was set to *random*. Released photons had a monochromatic *wavelength* (420 nm), with no secondary photons modelled. Corrections were used for strongly absorbing media, and reflections were counted. *Ray tracing* is *active* and *secondary photons* are capped at 1000 to prevent an inordinate number of photons from being generated by reflections. Photons undergoing total internal reflection (TIR) were not capped. Recorded outputs included the number of reflections of photons and the optical path length for each material used.

3. Experimental validation of FEA

To validate the model and to enable design choices, a series of flow cells of differing designs matching modelled dimensions were manufactured, and optical performance was assessed. A series of individual microfluidic channels were fabricated to compare the modelling results with an experimental workup. Flow cells with channel widths increasing by 0.1 mm between 0.3 and 0.8 mm were manufactured. Adding a mirror behind the transparent test chips also assessed the impact of adding a reflective channel coating. An analogous non-radioactive intermediate was used for photon production to assess the results from the numerical model without generating contaminated waste. The luminol-peroxide chemiluminescence (CL) reaction catalysed by the presence of cobalt (II) exhibits a predictable and repeatable production of light (420 nm); similar luminol-based detection systems have been employed in in situ analytical systems [60–63] and is an ideal candidate due to demonstrated consistent photon production at low sample volumes.

3.1. Materials

The luminol-cobalt solution was prepared by adding the following reagents to ultra-high purity water (UHP; 18.2 MΩ-cm), making up a total volume of 1 l; 0.27 g of analytical grade luminol (5-amino-2, 3-dihydro-, 4-phthalazinedione, Sigma-Aldrich, USA), 22 g of reagent grade potassium carbonate (Sigma-Aldrich, USA), 3.9 ml of Co(II) solution (1000 ppm standard in 2% by volume HNO_3, Certipur, Merck, Germany) and approximately 7 ml HCl 30% (Trace Metal grade, Fluka Analytical, Honeywell, USA) to adjust the pH of the solution to 10.2 for maximum chemiluminescence [63,64]. The solution was stored at approximately 6 ℃ in excess of 24 h to maximise luminol response [63, 64] then allowed to warm to room temperature by exposure to ambient temperature for 6–12 h prior to use.

Stock hydrogen peroxide (H_2O_2) (30% w/v ROMIL pure chemistry) was sequentially diluted to create working solutions of 0.01–0.001 M using deionised water. The use of narrow-necked, opaque high-density polyethylene (HDPE) sample bottles, aluminium foil shields over the apparatus, and reduced lighting in the laboratory minimised the potential for undesired photochemical reactions during reagent preparation and sample analysis.

3.2. Flow cell fabrication

The flow cells (Fig. 2) consisted of a single channel and were manufactured from PMMA (theplasticshop, UK) with cell channel widths ranging from 0.3 mm to 0.8 mm with inlet and outlet ports. The channel height remained the same for all flow cells (0.3 mm). The flow cells and channels were micro-milled (Datron Neo CNC, DATRON Dynamics, Inc, USA) and solvent polished to obtain high-quality optical surfaces [65].

3.3. Equipment

The flow system (Fig. 3) consisted of a peristaltic pump (Watson Marlow 520 SR peristaltic pump, Watson & Marlow Ltd, UK) used to propel the luminol solution and H_2O_2 reagent through the system. A 'T' mixer was used to mix the reagents. Teflon tubing (0.5 mm i.d. Merck, Germany) was used throughout the setup except for the peristaltic pump tubing (PVC Manifold 0.25 mm i.d. Watson & Marlow Ltd, UK).

Prior to use, both exterior sides of the flow cell were cleaned of contamination with isopropanol to improve optical transmittance and placed directly in front of the PMT (Hamamatsu H10492–011, Japan, which includes a 1 V/uA transimpedance amplifier) with a total distance of 2 mm between the channel and PMT window. The other side of the flow cell had an optical mirror positioned behind it, and the remaining sides and edges were painted over with black paint to prevent ambient light from entering or stray light from escaping. The flow cell and PMT were placed in a black foam box with the edges sealed with black tape. All exposed tubing was wrapped in black tape to prevent unwanted photochemical reactions of the reagents prior to reaching the flow cell and to prevent the Teflon tubing from acting as light guides towards the detector. A LabVIEW Analogue Digital Converter (DAQ NI USB-6001, LabView, UK) was used to collect the signal from the PMT and transmit the signal in volts to a laptop computer using LabVIEW 2016 with a signal collection rate of 10 Hz. The PMT was supplied with 11.5 V from an external power supply.

The volume of each flow cell resulted in different sample residence times (Table S.6). The residence time of each flow cell was calculated using the experimentally determined flow rate of 0.231 ml/min.

3.4. Optimisation and baseline determination

A range of H_2O_2 concentrations (6 from 0.001 to 0.01 M) and gain settings (from 0.60 V to 0.70 V by increments of 0.01 V) were trialled to find the optimum configuration to maximise signal output and reduce noise. For each H_2O_2 concentration, the optimal gain setting was also established; the H_2O_2 reaction was equilibrated for 3 min, and the gain setting was run for 3 min at each 0.01 V interval. Through this optimisation process, the optimal H_2O_2 concentration and gain settings for this study were established to be 0.002 M H_2O_2 and 0.66 V, respectively, for the specific equipment setup and reagent use.

Prior to each analysis, the manifold, including the flow cell, was cleaned internally by flushing with UHP water (2 mins), HCl (2 mins), and again UHP water (2 mins) to prevent HCl from adjusting the pH of the reagents from their buffered state (luminol will only emit light in its dissociated state [66]). Baseline output from the PMT was determined by running UHP water through the 0.6 mm flow cell for 5 mins at a flow rate of 0.231 ml/min after 5 mins of calibration time. The resulting background output of 0.53 V was subtracted from all experimentally obtained readings, and the subsequent limit of detection was established to be 0.05 V, calculated from the mean of triplicate standard deviations of background measurements.

3.5. Flow cell quality control and testing

Six flow cells were used in the experimental validation, each unique owing to its cell width or whether it used a mirrored or opaque base backing. At all times before reagents were introduced in the manifold, the flow cells and tubing were cleaned by pumping UHP water (up to 3 mins) followed by 0.1 M HCl (up to 3 mins) and then again flushed with UHP water (up to 3 mins). Flow cell channels were micrographed (Zeta-20 Profilometer, KLA, USA) before experimentation to confirm flow cell channel dimensions and check for potential milling defects or blockages. Each flow cell was checked for leaks by flushing through coloured dye before cleaning.

Flow cells were primed by running the reagents for 5 mins and then cleaned using the aforementioned method. For each flow cell, the reaction was left to equilibrate for 3 mins and then run for 3 mins following the reaction equilibration. This process was repeated twice for each flow cell to obtain triplicate results. This process was repeated for the opaque flow cells by removing the mirror and placing a piece of black electrical tape against the back of the flow cell.

4. Results & discussion

4.1. Modelled results: effect of dimensional properties

All results are assessed relative to a baseline to enable direct

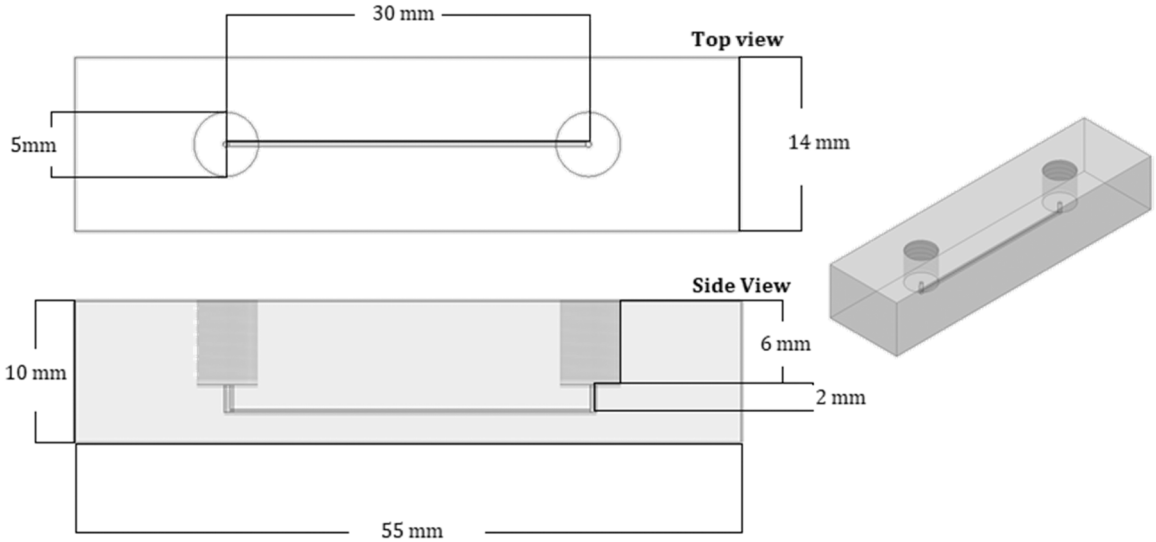

Fig. 2. Schematic presentation of flow cell size and dimensions including channel length, inlet port and outlet port (Autodesk Inventor).

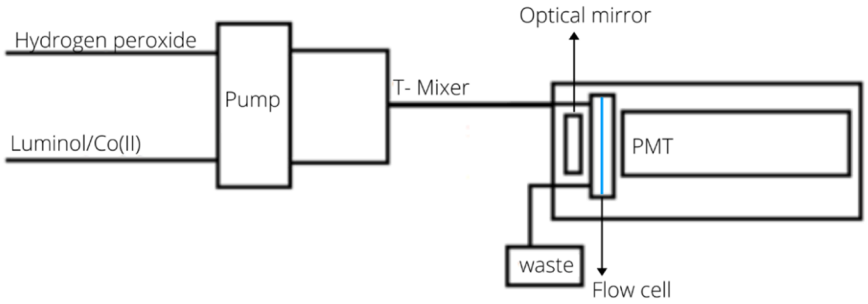

Fig. 3. Flow injection system for the chemiluminescence imaging of a flow cell.

comparisons across the modelled parameters. The baseline case has a channel width and height of 0.3 mm, length of 30 mm, and spacer thickness of 2 mm with an opaque backing. Results are considered in turn through the independent variation of one property, and the detector output was plotted as a function of microfluidic dimensional parameters, channel width, and height (Fig. 4). Each investigation has a 'reflective' and 'opaque' case for each dimension change.

Where channel width was increased, a positive linear correlation for both opaque and reflective channel cases was observed from channel width of 0.3–0.8 mm. Detector output in the opaque channel case increased 165% from the baseline case (1), whilst output in the reflective channel case was 220% higher than the baseline case (an increase of 200% over the reflective 0.3 mm width channel). When increasing channel height over a range of 0.3–0.8 mm, the detector output in the opaque channel linearly increased 146% from the baseline, whilst output in the reflective channel was 191% higher than the baseline case (an increase of 171% over the reflective 0.3 mm width and height channel). A wider microfluidic channel increased the surface area exposed to the detector and did not impact laminar flow with the dimensions modelled (Fig. 4a). However, a wider microfluidic channel increases the possibility for physical quenching within the channel, reducing the proportion of transmitted photons and does not compensate for reduced detector output in the absence of a reflective surface.

The flow cells with the largest volume were those with a height or width of 0.8 mm, both these flow cells contained an identical channel volume and number of emitted photons. The 0.8 mm channel height flow cell demonstrated 28% less detector output for the reflective case and 19% less for the opaque case relative to the 0.8 mm channel width flow cell. The increased distance (0.6 mm) travelled by the photons to the detecting face for the 0.8 mm channel height likely accounts for this decrease in detector output due to increased attenuation and geometrical losses. Additionally, in a wide and shallow channel, the photons are being released (on average) closer to the detecting face resulting in a greater number of photons reaching the detector, compared to a deep and thin channel which exhibits a decrease in overall detector output.

The static cross-sectional surface area (9 mm^2) exposed to the detector by the 0.8 mm channel height flow cell is less than the surface area (24 mm^2) exposed to the detector by the 0.8 mm channel width flow cell, indicating that photon attenuation through diffuse reflection, refraction, and absorption within the microfluidic channel contributes to loss of detector output.

The comparison between channel width and height establishes that increasing sample volume (number of photons emitted) is inadequate to compensate for the loss of photons through a reduction in the field of view towards the detector and attenuation processes in the channel's overall detector output. An additional component to the reduction in overall detector output is explained by the opaque PMMA's reflectivity coefficient (0.04) compared to that for the aluminium optical mirror (0.96). A more significant number of photons that fail to reach the detector are absorbed, refracted, and diffusely reflected throughout the channel and spacer in the opaque channels. Photons that interact with the opaque surface behind the channel results in the diffuse reflection of photons which transport less efficiently due to their lower energy and are attenuated more rapidly in the spacer. In comparison, photons that undergo specular reflection transport more efficiently through the system and are less likely to be attenuated in the spacer.

Two channel widths were explored, 0.3 mm and 0.6 mm, over different spacer thicknesses (0.5–4 mm) to examine the relationship

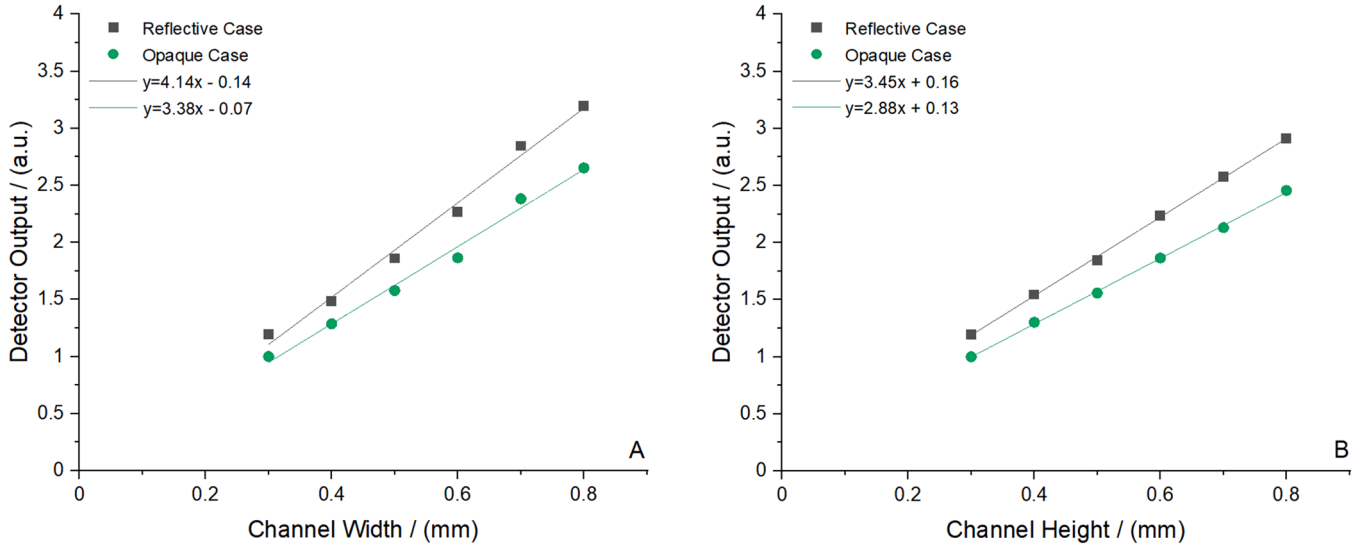

Fig. 4. Modelled detector output normalised to the opaque 0.3 mm channel width case and channel height for (a) changing channel width opaque channel produced $R^2 > 0.98$ and reflective channels produced $R^2 > 0.99$; (b) changing channel height, both opaque and reflective channels produced $R^2 > 0.99$.

between spacer thicknesses and channel width (Fig. 5). The number of photons released was scaled in proportion to each channel volume. Both 0.3 mm and 0.6 mm opaque and reflective models established a linear decrease in detector output over the spacer thicknesses explored. For the 0.6 mm channel width increasing the PMMA spacer thickness by 3.5 mm resulted in 63% less detector output in the opaque channel case and 70% less detector output for the reflective channel case (Fig. 5a). For the 0.3 mm channel width, the reflective and opaque cases, the increase of 3.5 mm in spacer thickness resulted in 25% less detector output for the opaque case and 27% less detector output for the reflective case (Fig. 5b). The general decrease in detector output can be attributed to several mechanisms of photon loss; increased photon attenuation in the thicker spacer prior to reaching the detector and photon loss due to geometry independent of photon attenuation in the spacer.

A parallel study was run to characterise the impact of geometrical losses on detector output. Spacer walls were set to detect the number of photons that hit the surface wall. Photon loss was reported as a ratio (Table S.7) of detector output for each case and was not normalised to the baseline case. The impact of geometrical losses of photons to spacer walls increased linearly with spacer thickness until 4 mm. This relationship then delineates into an exponential increase despite the surface area of the spacer walls increasing in regular 70 mm^2 increments. The maximum geometrical photon loss to spacer walls was 16% of the overall detector output for the 0.3 mm, 4 mm spacer reflective case. Attenuation is the dominant mechanism of photon loss in the system where the spacer thickness is increased.

The channel dimensions and the number of released releases remain constant for the 0.6 and 0.3 mm cases, respectively. The channel width has a demonstrable impact on detector output for both reflective and opaque causes but a more significant effect on the reflective case. When the channel width is 0.6 mm, the detector output is 130% more than the equivalent spacer thickness (0.5 mm) case at 0.3 mm for the reflective system (104% for the opaque system). These results determine that the model can simulate an increase in channel width to mitigate the effects of a thicker spacer. Increasing spacer thickness decreases detector output; ideally, the flow cell should be manufactured with the thinnest spacer possible whilst not compromising the bond quality between the two PMMA layers.

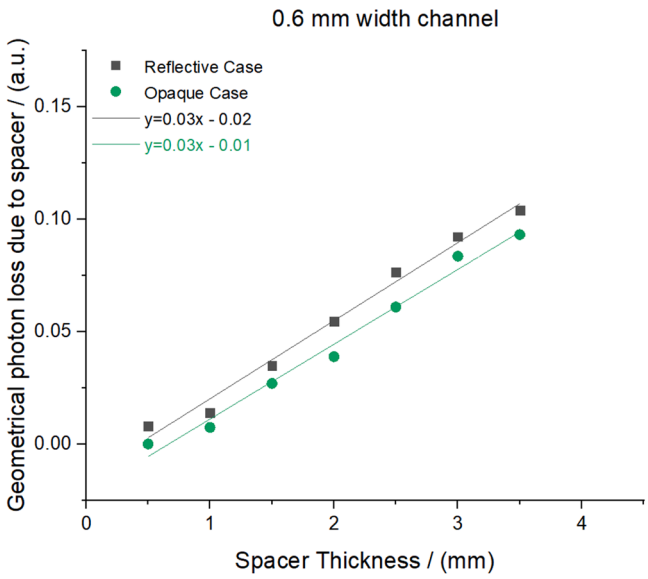

Fig. 6. Geometrical photon loss due to spacer plotted as a ratio to the detector output for each case spacer case. The ratio of photon loss was not normalised to the baseline case. Both opaque and reflective systems producing $R^2 > 0.98$.

4.2. *Modelled results: effect of reflective material properties*

A study was performed using fixed values for channel volume and dimensions exposed to the detector to isolate the impact of a reflective plane on detector output. The baseline channel, spacer, and detector conditions were used. In this study, released photons were increased linearly, and the reflective coating was adjusted independently to assess the impact of each reflective pane on detector output. In Fig. 7, the perfect reflector (reflectivity coefficient of 1) demonstrated a detector output 208% higher than the baseline case (1), and the gold foil (0.40 reflectivity coefficient) demonstrated detector output 174% higher than the baseline case. The opaque PMMA (reflectivity coefficient of 0.04) surface demonstrated a detector output increase of 153% from the baseline, demonstrating the uniform material absorbance in the model and the importance of incorporating a reflective surface.

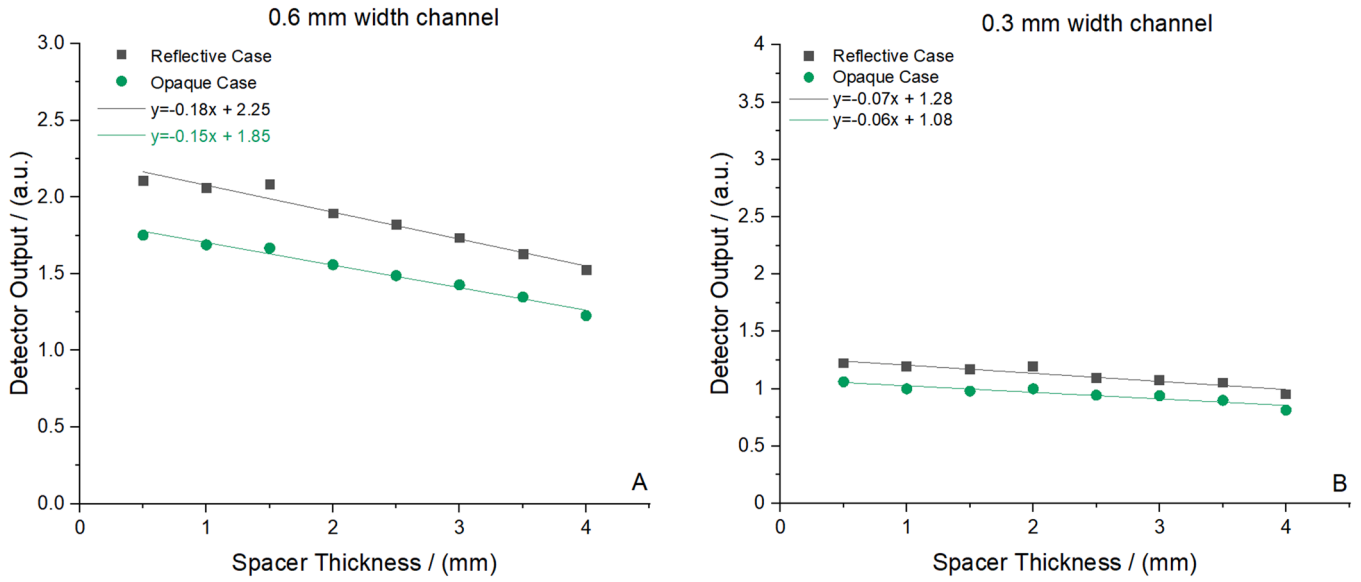

Fig. 5. Modelled detector output normalised to the 0.3 mm width and height opaque channel case. 0.6 mm channel width opaque results producing $R^2 > 0.98$ and reflective results producing $R^2 > 0.96$ (a), 0.3 mm channel width, opaque results producing $R^2 > 0.87$ and reflective results producing $R^2 > 0.88$ (b) for increasing spacer thickness from 0.5 mm to 4 mm.

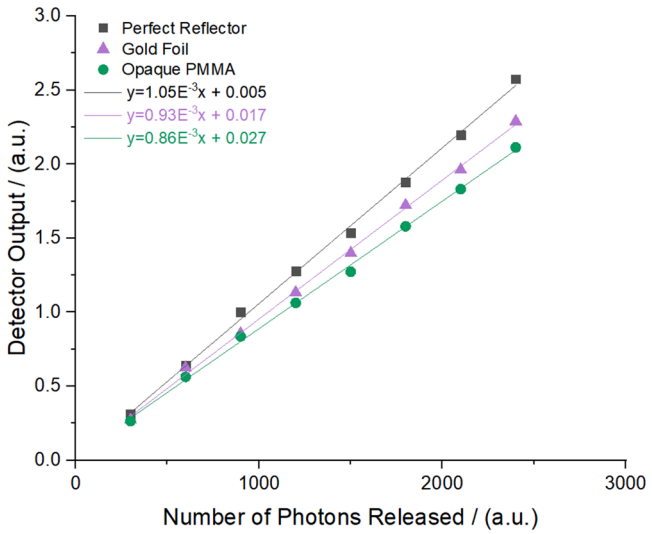

Fig. 7. Modelled increasing the number of photons released cases for different reflective channel coatings and. The number of photons released was increased proportionally. All cases were normalised to the opaque baseline case. All results produced $R^2 > 0.99$.

4.3. Experimental validation of the model

The outcomes of FEA were validated against analogous experiments to compare and quantify any parameters that could not be modelled. The data is a mean average of triplicates, and three groups of repeated experiments were used to obtain the error bars. The error bars were generated from a combined standard deviation of the triplicate readings and are reported relative to the baseline. Flow cell residence times were calculated experimentally based on channel width and volume (Table S.6.) All results (Fig. 8) are reported as a ratio normalised to the result obtained from the baseline case.

A correlation between the FEA models and experimentally derived values results were obtained (Fig. 8). Relative differences in detector output between modelled and experimental opaque and reflective systems are attributed to variation in extrinsic absorption, scattering, and refraction mechanisms in the experimental setup, which are currently not possible to account for entirely in the modelled system. The impact of these processes is most significant for the reflective system because of the increased number of photon reflections and potential photon trajectories. However, the general increase in photon trajectories toward the detector results in higher overall detector output than the equivalent opaque system.

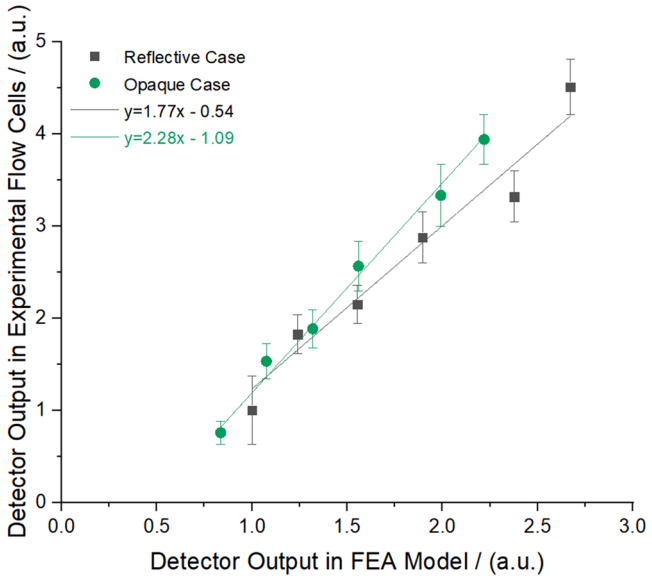

Fig. 8. Comparison of modelled and experimental detector outputs of reflective and opaque cases. Linear regression has been applied to 6 points of the graph to demonstrate correlation between experimental and modelled results. Opaque results produced $R^2 > 0.99$ and reflective case results produced $R^2 > 0.95$.

The difference in error bar size and associated uncertainty of the experimental system can also be accounted for through several processes; tool marks from milling resistant to solvent polishing, inconsistencies in pump speed and absorption mechanisms such as extrinsic impurities and ion scattering caused by microscopic quantities of metallic ions. The greater variation between error bars for smaller channel widths can also result from reduced flow cell residence time and smaller sample volumes where variation in reagent composition and resultant light output has a greater impact on detector output. The flushing of 0.1 M HCl limited the presence of metal ions, but this process may have contributed to the hydrolysis of PMMA's ester group to an alcohol. This process can potentially increase photon attenuation due to hydrogen effects and extrinsic ion absorption if the alcohol group is deprotonated. Besides the expected reduction in detector output for the opaque system, the theoretical and experimental values agree within the opaque and reflective systems.

5. Conclusions

Optimisation based design methodology for the numerical modelling of LoC Systems designed to detect pure β-emitting radionuclides has been presented. Numerical analysis has evaluated different bulk design features on photon transmission and detection. This numerical analysis has been experimentally validated as a method for inexpensive, rapid prototyping of bulk optical parameters. Results demonstrated that parameters that increased surface area exposed to the detector and reflective planes had the most significant impacts on increasing detector output and that crude design assumptions (such as increasing volume by increasing channel height) should not be relied on for increasing detector output. Initial findings suggest a maximum spacer thickness of 3 mm and a wide but flat channel that can expose the maximum surface area to the detector but still maintain the benefits associated with microfluidic systems. Work to date has demonstrated the value of FEA modelling in directing areas for development and optimised solutions for rapid prototyping of radiometric LoCs. This method provides potential translation to other microfluidic systems that rely on direct photon detection, highlighting the most promising novel designs for development—reducing material consumption and requirement for specialist facilities needed for handling radioactive materials during the prototyping process.

From a practical perspective, integrating an LoC system with a detector will require consideration of elements not accounted for in this computational and experimental study. Although we have presented design information for several cases, this paper has not considered the impact of radioactive decay kinetics or quenching on the transmittance of photons through a modelled or experimental microfluidic system. Depending on the size and activity of the sample that the flow cell can accommodate, these factors may require compromises and the lengths of the channels required for separation or extraction to ameliorate these issues.

The preferred development areas relate to validating the experimental and modelled results using a pure β-emitting radionuclide. In radiochemistry, developed microsystems are coupled to spectrometers for elemental or isotopic analyses; therefore, effort should focus on integrating detection and measurement directly in the LoC, leading to a considerable decrease in the volumes of samples and reagents. Microfluidic tools already significantly reduce analytical effluent generated by the methods currently used in laboratories; implementing parallelizable and automated sample preparation methods will continue to reduce this

further. The findings of the modelled and experimental results demonstrate that the potential of a new best practice for designing and prototyping radiochemical LoC platforms is not only viable but crucial to establishing best practice guidelines for novel prototypes.

CRediT authorship contribution statement

Sarah E. Lu: Conceptualization, Methodology, Software, Writing – original draft, Data curation, Formal analysis. **Andrew Morris**: Supervision, Methodology, Validation. **Geraldine Clinton-Bailey**: Supervision, Methodology, Writing – review & editing. **Medya Namiq**: Methodology, Software. **Paul C. Gow**: Methodology. **Antony Birchill**: Methodology. **Sebastian Steigenberger**: Methodology, Resources. **James Wyatt**: Methodology. **Reuben Forrester**: Methodology. **Matthew Mowlem**: Reviewing, Editing, Resources. **Phillip, E. Warwick**: Supervision, Reviewing, Editing.

Declaration of Competing Interest

The authors declare that they have no known competing financial interests or personal relationships that could have appeared to influence the work reported in this paper.

Data availability

Data will be made available on request.

Acknowledgements

This work was supported by the Natural Environmental Research Council [grant number NE/N012070/1].

Appendix A. Supporting information

Supplementary data associated with this article can be found in the online version at doi:10.1016/j.sna.2023.114496.

References

[1] H. Kawamura, H. Hirano, Y. Katsumura, S. Uchida, T. Mizuno, H. Kitajima, Y. Tsuzuki, T. Terachi, M. Nagase, N. Usui, J. Takagi, H. Urata, Y. Shoda, T. Nishimura, BWR water chemistry guidelines and PWR primary water chemistry guidelines in Japan – Purpose and technical background, Nucl. Eng. Des. 309 (2016) 161–174, https://doi.org/10.1016/j.nucengdes.2016.08.029.

[2] P. Gaca, D. Reading, P. Warwick, Application of multiple quench parameters for confirmation of radionuclide identity in radioanalytical quality control, J. Radioanal. Nucl. Chem. 322 (2019) 1383–1390, https://doi.org/10.1007/s10967-019-06788-z.

[3] P.E. Warwick, I.W. Croudace, Rapid on-site radionuclide screening of aqueous waste streams using dip-stick technologies and liquid scintillation counting, J. Radioanal. Nucl. Chem. 314 (2017), https://doi.org/10.1007/s10967-017-5413-9.

[4] A.M. Nightingale, A.D. Beaton, M.C. Mowlem, Trends in microfluidic systems for in situ chemical analysis of natural waters, Sens. Actuators.: B. Chem. 221 (2015) 1398–1405, https://doi.org/10.1016/j.snb.2015.07.091.

[5] V. Arima, G. Pascali, O. Lade, H.R. Kretschmer, I. Bernsdorf, V. Hammond, P. Watts, F. De Leonardis, M.D. Tarn, N. Pamme, B.Z. Cvetkovic, P.S. Dittrich, N. Vasovic, R. Duane, A. Jaksic, A. Zacheo, A. Zizzari, L. Marra, E. Perrone, P. A. Salvadori, R. Rinaldi, Radiochemistry on chip: Towards dose-on-demand synthesis of PET radiopharmaceuticals, Lab a Chip 13 (2013) 2328–2336, https://doi.org/10.1039/c3lc00055a.

[6] S. Lu, A.M. Giamis, V.W. Pike, Synthesis of [18F]Fallypride in a Micro-Reactor: Rapid Optimization and Multiple-Production in Small Doses for Micro-PET Studies, Curr. Radiopharm. 2 (2009) 49–55.

[7] J. Wang, P.H. Chao, R.M.Van Dam, Ultra-compact, automated microdroplet radiosynthesizer, Lab a Chip 19 (2019) 2415–2424, https://doi.org/10.1039/c9lc00438f.

[8] M. Sergeev, M. Lazari, F. Morgia, J. Collins, M.R. Javed, O. Sergeeva, J. Jones, M. E. Phelps, J.T. Lee, P.Y. Keng, R.M. van Dam, Performing radiosynthesis in microvolumes to maximize molar activity of tracers for positron emission tomography, Commun. Chem. 1 (2018) 1–10, https://doi.org/10.1038/s42004-018-0009-z.

[9] S. Sadeghi, V. Liang, S. Cheung, S. Woo, C. Wu, J. Ly, Y. Deng, M. Eddings, R. M. van Dam, Reusable electrochemical cell for rapid separation of [18F]fluoride from [18O]water for flow-through synthesis of 18F-labeled tracers, Appl. Radiat. Isot. 75 (2013) 85–94, https://doi.org/10.1016/J.APRADISO.2012.12.021.

[10] A.A. Dooraghi, P.Y. Keng, S. Chen, M.R. Javed, C.-J. "C.J." Kim, A. F. Chatziioannou, R.M. van Dam, Optimization of microfluidic PET tracer synthesis with Cerenkov imaging, Analyst 138 (2013) 5654, https://doi.org/10.1039/c3an01113e.

[11] A.I. Anzellotti, A.R. McFarland, D. Ferguson, K.F. Olson, Towards the Full Automation of QC Release Tests for [18F]fluoride-labeled Radiotracers, Curr. Org. Chem. 17 (2013) 2153–2158.

[12] M.D. Tarn, D. Maneuski, R. Alexander, N.J. Brown, V. O'shea, S.L. Pimlott, N. Pamme, S.J. Archibald, Positron detection in silica monoliths for miniaturised quality control of PET radiotracers, Chem. Commun. 52 (2016) 7221, https://doi.org/10.1039/c6cc00660d.

[13] M.P. Taggart, M.D. Tarn, M.M.N. Esfahani, D.M. Schofield, N.J. Brown, S. J. Archibald, T. Deakin, N. Pamme, L.F. Thompson, Development of radiodetection systems towards miniaturised quality control of PET and SPECT radiopharmaceuticals, Lab a Chip 16 (2016) 1605–1616, https://doi.org/10.1039/c6lc00099a.

[14] M.P. Taggart, M.D. Tarn, M.M.N. Esfahani, S.J. Archibald, T. Deakin, N. Pamme, L. F. Thompson, On-chip detection of radioactivity via silicon-based sensors for the quality control testing of radiopharmaceuticals, MicroTAS 2015 - 19th International Conference on Miniaturized Systems for Chemistry and Life Sciences. (2015).

[15] Z. Liu, X. Lan, Microfluidic radiobioassays: A radiometric detection tool for understanding cellular physiology and pharmacokinetics, Lab a Chip 19 (2019) 2315–2339, https://doi.org/10.1039/c9lc00159j.

[16] A.G. Servis, T. Parsons-Davis, K.J. Moody, N. Gharibyan, 3D printed microfluidic supported liquid membrane module for radionuclide separations, Ind. Eng. Chem. Res. 60 (2021) 629–638, https://doi.org/10.1021/acs.iecr.0c05349.

[17] G. Hellé, C. Mariet, G. Cote, Microfluidic tools for the liquid-liquid extraction of radionuclides in analytical procedures, Procedia Chem. 7 (2012) 679–684, https://doi.org/10.1016/j.proche.2012.10.103.

[18] S. Rassou, C. Mariet, T. Vercouter, Analysis of radionuclides in microsystem: application to the selective recovery of 55Fe by solvent extraction, EPJ Nuclear, Sci. Technol. 6 (2020) 10, https://doi.org/10.1051/epjn/2020002.

[19] C. Rensch, S. Lindner, R. Salvamoser, S. Leidner, C. Böld, V. Samper, D. Taylor, M. Baller, S. Riese, P. Bartenstein, C. Wängler, B. Wängler, A solvent resistant lab-on-chip platform for radiochemistry applications, Lab a Chip 14 (2014) 2556–2564, https://doi.org/10.1039/c4lc00076e.

[20] N.S. Ha, S. Sadeghi, R.M. van Dam, Recent progress toward microfluidic quality control testing of radiopharmaceuticals, Micromachines 8 (2017) 3–7, https://doi.org/10.3390/mi8110337.

[21] A.M. Elizarov, Microreactors for radiopharmaceutical synthesis, Lab a Chip 9 (2009) 1326–1333, https://doi.org/10.1039/b820299k.

[22] P.Y. Keng, R.M. van Dam, Digital Microfluidics: A New Paradigm for Radiochemistry, Molecular Imaging. 14 (2015) 7290.2015.00030. https://doi.org/10.2310/7290.2015.00030.

[23] P. Watts, G. Pascali, P.A. Salvadori, Positron emission tomography radiosynthesis in microreactors, J. Flow. Chem. 2 (2012) 37–42, https://doi.org/10.1556/jfc-d-12-00010.

[24] P.W. Miller, A.J. deMello, A.D. Gee, Application of Microfluidics to the Ultra-Rapid Preparation of Fluorine-18 Labelled Compounds, Current Radiopharmaceuticals. 3, 2010: 254–262.

[25] C. Rensch, A. Jackson, S. Lindner, R. Salvamoser, V. Samper, S. Riese, P. Bartenstein, C. Wängler, B. Wängler, Microfluidics: A Groundbreaking Technology for PET Tracer Production, Molecules 18 (2013) 7930–7956, https://doi.org/10.3390/molecules18077930.

[26] A.Y. Lebedev, 17 - Microfluidic devices for radio chemical synthesis, in: X. (James) Li, Y. Zhou (Eds.), Microfluidic Devices for Biomedical Applications, Woodhead Publishing, 2013: pp. 594–633. https://doi.org/10.1533/9780857097040.4.594.

[27] G. Pascali, P. Watts, P.A. Salvadori, Microfluidics in radiopharmaceutical chemistry, Nucl. Med. Biol. 40 (2013) 776–787, https://doi.org/10.1016/j.nucmedbio.2013.04.004.

[28] C. Mariet, A. Vansteene, M. Losno, J. Pellé, J.-P. Jasmin, A. Bruchet, G. Hellé, Microfluidics devices applied to radionuclides separation in acidic media for the nuclear fuel cycle, Micro Nano Eng. 3 (2019) 7–14, https://doi.org/10.1016/j.mne.2019.02.006.

[29] J.S. Cho, R. Taschereau, S. Olma, K. Liu, Y.C. Chen, C.K.F. Shen, R.M. Van Dam, A. F. Chatziioannou, Cerenkov radiation imaging as a method for quantitative measurements of beta particles in a microfluidic chip, Phys. Med. Biol. 54 (2009) 6757–6771, https://doi.org/10.1088/0031-9155/54/22/001.

[30] M.D. Tarn, N.Y. Kızılyer, M.M.N. Esfahani, P. Joshi, N.J. Brown, N. Pamme, D. G. Jenkins, S.J. Archibald, Plastic Scintillator-Based Microfluidic Devices for Miniaturized Detection of Positron Emission Tomography Radiopharmaceuticals, Chem. - A Eur. J. 24 (2018) 13749–13753, https://doi.org/10.1002/chem.201802395.

[31] A. Mapelli, B. Gorini, M. Haguenauer, S. Jiguet, G.L. Miotto, W. Vandelli, N. V. Triviño, P. Renaud, Scintillation particle detection based on microfluidics, Sens. Actuators A: Phys. 162 (2010) 272–275, https://doi.org/10.1016/J.SNA.2010.03.040.

[32] P. Maoddi, A. Mapelli, P. Bagiacchi, B. Gorini, M. Haguenauer, G.L. Miotto, R. M. Garcia, F.S. Tehrani, S. Veneziano, P. Renaud, Scintillation detectors based on silicon microfluidic channels, C01019–C01019, J. Instrum. 9 (2014), https://doi.org/10.1088/1748-0221/9/01/C01019.

[33] Y. Mishnayot, M. Layani, I. Cooperstein, S. Magdassi, G. Ron, Three-dimensional printing of scintillating materials, Charact. Plast. Scintill. J. Chem. Phys. 85 (2014) 801, https://doi.org/10.1063/1.4891703.
[34] R. Merín, A. Tarancón, K. Mitev, S. Georgiev, C. Dutsov, H. Bagán, J.F. García, Evaluation of synthesis conditions for plastic scintillation foils used to measure alpha- and beta-emitting radionuclides, J. Radioanal. Nucl. Chem. 319 (2019) 135–145, https://doi.org/10.1007/s10967-018-6341-z.
[35] J.S. Cho, R. Taschereau, S. Olma, K. Liu, Y.C. Chen, C.K.F. Shen, R.M. Van Dam, A. F. Chatziioannou, Cerenkov radiation imaging as a method for quantitative measurements of beta particles in a microfluidic chip, Phys. Med. Biol. 54 (2009) 6757–6771, https://doi.org/10.1088/0031-9155/54/22/001.
[36] B.J. Beattie, D.L.J. Thorek, C.R. Schmidtlein, K.S. Pentlow, J.L. Humm, A. H. Hielscher, Quantitative Modeling of Cerenkov Light Production Efficiency from Medical Radionuclides, PLoS ONE 7 (2012), e31402, https://doi.org/10.1371/journal.pone.0031402.
[37] J.S. Cho, N.T. Vu, Y.H. Chung, Z.T. Yu, R.W. Silverman, R. Taschereau, H.R. Tseng, A.F. Chatziioannou, Detection of Beta Particles in a Microfluidic Chip Using a Scintillator and CCD, in: 2006 IEEE Nuclear Science Symposium Conference Record, IEEE, 2006: pp. 1977–1981. https://doi.org/10.1109/NSSMIC.2006.354301.
[38] S. Agostinelli, J. Allison, K. Amako, J. Apostolakis, H. Araujo, P. Arce, M. Asai, D. Axen, S. Banerjee, G. Barrand, F. Behner, L. Bellagamba, J. Boudreau, L. Broglia, A. Brunengo, H. Burkhardt, S. Chauvie, J. Chuma, R. Chytracek, G. Cooperman, G. Cosmo, P. Degtyarenko, A. Dell'Acqua, G. Depaola, D. Dietrich, R. Enami, A. Feliciello, C. Ferguson, H. Fesefeldt, G. Folger, F. Foppiano, A. Forti, S. Garelli, S. Giani, R. Giannitrapani, D. Gibin, J.J. Gómez Cadenas, I. González, G. Gracia Abril, G. Greeniaus, W. Greiner, V. Grichine, A. Grossheim, S. Guatelli, P. Gumplinger, R. Hamatsu, K. Hashimoto, H. Hasui, A. Heikkinen, A. Howard, V. Ivanchenko, A. Johnson, F.W. Jones, J. Kallenbach, N. Kanaya, M. Kawabata, Y. Kawabata, M. Kawaguti, S. Kelner, P. Kent, A. Kimura, T. Kodama, R. Kokoulin, M. Kossov, H. Kurashige, E. Lamanna, T. Lampén, V. Lara, V. Lefebure, F. Lei, M. Liendl, W. Lockman, F. Longo, S. Magni, M. Maire, E. Medernach, K. Minamimoto, P. Mora de Freitas, Y. Morita, K. Murakami, M. Nagamatu, R. Nartallo, P. Nieminen, T. Nishimura, K. Ohtsubo, M. Okamura, S. O'Neale, Y. Oohata, K. Paech, J. Perl, A. Pfeiffer, M.G. Pia, F. Ranjard, A. Rybin, S. Sadilov, E. Di Salvo, G. Santin, T. Sasaki, N. Savvas, Y. Sawada, S. Scherer, S. Sei, V. Sirotenko, D. Smith, N. Starkov, H. Stoecker, J. Sulkimo, M. Takahata, S. Tanaka, E. Tcherniaev, E. Safai Tehrani, M. Tropeano, P. Truscott, H. Uno, L. Urban, P. Urban, M. Verderi, A. Walkden, W. Wander, H. Weber, J.P. Wellisch, T. Wenaus, D.C. Williams, D. Wright, T. Yamada, H. Yoshida, D. Zschiesche, Geant4—a simulation toolkit, Nuclear Instruments and Methods in Physics Research Section A: Accelerators, Spectrometers, Detectors and Associated Equipment. 506 (2003) 250–303. https://doi.org/10.1016/S0168–9002(03)01368–8.
[39] M. Pineda, P. Angeli, T. Tsukahara, E.S. Fraga, Modelling of Microfluidic Devices for Analysis of Radionuclides, in: A.A. Kiss, E. Zondervan, R. Lakerveld, L. Özkan (Eds.), Computer Aided Chemical Engineering, Elsevier, 2019: pp. 1807–1812. https://doi.org/10.1016/B978–0-12–818634-3.50302–7.
[40] M. Pineda, D. Tsaoulidis, P.I.O. Filho, T. Tsukahara, P. Angeli, E.S. Fraga, Design optimization of microfluidic-based solvent extraction systems for radionuclides detection, Nucl. Eng. Des. 383 (2021), 111432, https://doi.org/10.1016/j.nucengdes.2021.111432.
[41] G. Hellé, S. Roberston, S. Cavadias, C. Mariet, G. Cote, Toward numerical prototyping of labs-on-chip: modeling for liquid–liquid microfluidic devices for radionuclide extraction, Microfluid Nanofluid 19 (2015) 1245–1257, https://doi.org/10.1007/s10404-015-1643-8.
[42] D.Di Carlo, Inert. Microfluid. (2009), https://doi.org/10.1039/b912547g.
[43] E.L. Tóth, E. Holczer, P. Földesy, K. Iván, P. Fürjes, Microfluidic Particle Sorting System for Environmental Pollution Monitoring Applications, in: Procedia Engineering, Elsevier Ltd, 2016, pp. 1462–1465, https://doi.org/10.1016/j.proeng.2016.11.420.
[44] J. Zhou, P. Mukherjee, H. Gao, Q. Luan, I. Papautsky, Label-free microfluidic sorting of microparticles, APL Bioeng. 3 (2019), 041504, https://doi.org/10.1063/1.5120501.
[45] D. Huang, J. Man, D. Jiang, J. Zhao, N. Xiang, Inertial microfluidics: Recent advances, ELECTROPHORESIS 41 (2020) 2166–2187, https://doi.org/10.1002/elps.202000134.
[46] M.F. L'Annunziata, Chapter 16 - Cherenkov Radiation, in: M.F. L'Annunziata (Ed.), Radioactivity (Second Edition), Elsevier, Boston, 2016: pp. 547–581. https://doi.org/10.1016/B978–0-444–63489-4.00016–2.
[47] A. Mapelli, B. Gorini, M. Haguenauer, S. Jiguet, P. Renaud, Development and studies of a novel microfabricated radiation hard scintillation particle detector with high spatial resolution, 2009. https://doi.org/10.1016/j.nuclphysbps.2009.10.031.
[48] B. Alessandro Mapelli, Gorini Maurice Haguenauer, N. Sébastien Jiguet, Vico Triviño, Philippe Renaud, Novel radiation hard microfabricated scintillation detectors with high spatial resolution, Nucl. Instrum. Methods Phys. Res. Sect. A-Accel. Spectrometers Detect. Assoc. Equip. (2010), https://doi.org/10.1016/j.nima.2009.06.091.
[49] M. Mirasoli, M. Guardigli, E. Michelini, A. Roda, Recent advancements in chemical luminescence-based lab-on-chip and microfluidic platforms for bioanalysis, J. Pharm. Biomed. Anal. 87 (2014) 36–52, https://doi.org/10.1016/j.jpba.2013.07.008.
[50] H. Ben-Yoav, T. Elad, O. Shlomovits, S. Belkin, Y. Shacham-Diamand, Optical modeling of bioluminescence in whole cell biosensors, Biosens. Bioelectron. 24 (2009) 1969–1973, https://doi.org/10.1016/j.bios.2008.10.035.
[51] H.-F. Tsai, Y.-C. Tsai, S. Yagur-Kroll, N. Palevsky, S. Belkin, J.-Y. Cheng, Water pollutant monitoring by a whole cell array through lens-free detection on CCD, Lab Chip 15 (2015) 1472–1480, https://doi.org/10.1039/C4LC01189A.
[52] A. Lopreside, M.M. Calabretta, L. Montali, M. Zangheri, M. Guardigli, M. Mirasoli, E. Michelini, Bioluminescence goes portable: recent advances in whole-cell and cell-free bioluminescence biosensors, Luminescence 36 (2021) 278–293, https://doi.org/10.1002/bio.3948.
[53] V. Ivanov, A. Barnyakov, M. Barnyakov, V. Bobrovnikov, I. Ovtin, Numerical simulation of fast photo detectors based on microchannel plates, P09024–P09024, J. Instrum. 12 (2017), https://doi.org/10.1088/1748-0221/12/09/P09024.
[54] R.M. Winz, W. Wiechert, E. Von Lieres, Surface bound adsorption in a microfluidic T-sensor: Numerical comparison and optimization of 2D and 3D models and of sensor designs, in: Sensors and Actuators, B: Chemical, Elsevier, 2012: pp. 75–81. https://doi.org/10.1016/j.snb.2011.01.057.
[55] M. Yew, Y. Ren, K.S. Koh, C. Sun, C. Snape, A Review of State-of-the-Art Microfluidic Technologies for Environmental Applications: Detection and Remediation, Glob. Chall. 3 (2019) 1800060, https://doi.org/10.1002/gch2.201800060.
[56] L. Wolska, A. Sagajdakow, A. Kuczyńska, J. Namieśnik, Application of ecotoxicological studies in integrated environmental monitoring: Possibilities and problems, TrAC - Trends Anal. Chem. 26 (2007) 332–344, https://doi.org/10.1016/j.trac.2006.11.012.
[57] M.M. Calabretta, A. Lopreside, L. Montali, M. Zangheri, L. Evangelisti, M. D'Elia, E. Michelini, Portable light detectors for bioluminescence biosensing applications: A comprehensive review from the analytical chemist's perspective, Anal. Chim. Acta 1200 (2022), 339583, https://doi.org/10.1016/j.aca.2022.339583.
[58] COMSL Multiphysics®, (n.d.).
[59] COMSOL, Ray Optics Module Users Guide, (n.d.). https://doc.comsol.com/5.3/doc/com.comsol.help.roptics/RayOpticsModuleUsersGuide.pdf (accessed July 3, 2022).
[60] K. Okamura, H. Kimoto, K. Saeki, J. Ishibashi, H. Obata, M. Maruo, T. Gamo, E. Nakayama, Y. Nozaki, Development of a deep-sea in situ Mn analyzer and its application for hydrothermal plume observation, Mar. Chem. 76 (2001) 17–26, https://doi.org/10.1016/S0304-4203(01)00043-3.
[61] C. Provin, T. Fukuba, K. Okamura, T. Fujii, An integrated microfluidic system for manganese anomaly detection based on chemiluminescence: Description and practical use to discover hydrothermal plumes near the Okinawa trough, IEEE J. Ocean. Eng. 38 (2013) 178–185, https://doi.org/10.1109/JOE.2012.2208849.
[62] T. Doi, M. Takano, K. Okamura, T. Ura, T. Gamo, In-situ survey of nanomolar manganese in seawater using an autonomous underwater vehicle around a volcanic crater at Teishi Knoll, Sagami Bay, Japan, J. Oceanogr. 64 (2008) 471–477, https://doi.org/10.1007/s10872-008-0040-2.
[63] K. Okamura, T. Gamo, H. Obata, E. Nakayama, H. Karatani, Y. Nozaki, Selective and sensitive determination of trace manganese in sea water by flow through technique using luminol–hydrogen peroxide chemiluminescence detection, Anal. Chim. Acta 377 (1998) 125–131, https://doi.org/10.1016/S0003-2670(98)00617-5.
[64] J. Yuan, A.M. Shiller, Determination of Subnanomolar Levels of Hydrogen Peroxide in Seawater by Reagent-Injection Chemiluminescence Detection, Environ. Sci. Technol. 36 (1999) 393–396, https://doi.org/10.1021/ac981357c.
[65] I. Ogilvie, V. Sieben, C.F. Floquet, R. Zmijan, M. Mowlem, H. Morgan, Solvent processing of PMMA and COC chips for bonding devices with optical quality surfaces, 14th International Conference on Miniaturized System for Chemistry and Life Sciences. 1244–1246 (2010).
[66] L. Erdey, I. Buzás, K. Vigh, Luminol as a fluorescent acid-base indicator, Talanta 13 (1966) 463–469, https://doi.org/10.1016/0039-9140(66)80064-4.

Sarah E. Lu is a Postgraduate research student at the University of Southampton.

Dr Andrew Morris is a researcher in Ultra Miniature Environmental Sensors at the National Oceanography centre.

Dr Geraldine Clinton Bailey holds a PhD in situ dissolved uranium measurement techniques and has worked on the development of analytical techniques in the marine and environmental sciences with a focus on water quality and trace element analysis at the National Oceanography Centre

Dr Medya Namiq held a research engineer position, In-Situ Sensors at the National Oceanography Centre at the time of this work and is now a laser development engineer at TRUMPF.

Dr Paul C Gow is a senior research fellow at the University of Southampton in the Photonic systems circuits and sensors group.

Dr Antony Birchill, works n the Chief Scientist Group within the Environment Agency, during the time of this work he as a Research Engineer developing and deploying microfluidic sensors to determine nutrient concentrations in rivers, estuaries, coastal seas and the open ocean at the National Oceanography Centre

Dr Sebastian Steigenberger's work focuses on developing a method for the detection of dissolved organic nutrients (DON, DOP) for a lab on a chip (LOC) application at the National Oceanography Centre

James Wyatt is a research engineer at the National Oceanography Centre

Reuben Forrester is a research engineer at the National Oceanography Centre

Professor Matthew Mowlem is aPrincipal Investigator in the Ocean Technology and Engineering Group Principal Investigator at the National Oceanography Centre, UK

Prof Phil Warwick is Professor of Radioanalytical Chemistry at the University of Southampton, director of the commercial radioanalytical and consultancy laboratory, GAU-Radioanalytical and director of the NNUF – EXACT facility.